The FEBS Journal

FEBS PRESS science publishing by scientists

The effect of Mg^{2+} on Ca^{2+} binding to cardiac troponin C in hypertrophic cardiomyopathy associated *TNNC1* variants

Kaveh Rayani[1], Eric R. Hantz[2], Omid Haji-Ghassemi[3], Alison Y. Li[1], Anne M. Spuches[4], Filip Van Petegem[3], R. John Solaro[5], Steffen Lindert[2] and Glen F. Tibbits[1,6,7]

1 Molecular Cardiac Physiology Group, Simon Fraser University, Burnaby, Canada
2 Department of Chemistry and Biochemistry, Ohio State University, Columbus, OH, USA
3 Department of Biochemistry and Molecular Biology, The University of British Columbia, Vancouver, Canada
4 Department of Chemistry, 300 Science and Technology, East Carolina University, Greenville, NC, USA
5 Department of Physiology and Biophysics and the Center for Cardiovascular Research, College of Medicine, University of Illinois at Chicago, USA
6 Department of Molecular Biology and Biochemistry, Simon Fraser University, Burnaby, Canada
7 BC Children's Hospital Research Institute, Vancouver, Canada

Keywords
calorimetry; ITC; MD simulation; molecular dynamics; myofilament; thermodynamic integration

Correspondence
G. F. Tibbits, BC Children's Hospital Research Institute, Vancouver, BC V5Z 4H4, Canada
Tel: +1 604 910 4358
E-mail: tibbits@sfu.ca

(Received 29 December 2021, revised 14 May 2022, accepted 13 July 2022)

doi:10.1111/febs.16578

Cardiac troponin C (cTnC) is the critical Ca^{2+}-sensing component of the troponin complex. Binding of Ca^{2+} to cTnC triggers a cascade of conformational changes within the myofilament that culminate in force production. Hypertrophic cardiomyopathy (HCM)-associated *TNNC1* variants generally induce a greater degree and duration of Ca^{2+} binding, which may underly the hypertrophic phenotype. Regulation of contraction has long been thought to occur exclusively through Ca^{2+} binding to site II of cTnC. However, work by several groups including ours suggest that Mg^{2+}, which is several orders of magnitude more abundant in the cell than Ca^{2+}, may compete for binding to the same cTnC regulatory site. We previously used isothermal titration calorimetry (ITC) to demonstrate that physiological concentrations of Mg^{2+} may decrease site II Ca^{2+}-binding in both N-terminal and full-length cTnC. Here, we explore the binding of Ca^{2+} and Mg^{2+} to cTnC harbouring a series of *TNNC1* variants thought to be causal in HCM. ITC and thermodynamic integration (TI) simulations show that A8V, L29Q and A31S elevate the affinity for both Ca^{2+} and Mg^{2+}. Further, L48Q, Q50R and C84Y that are adjacent to the EF hand binding motif of site II have a more significant effect on affinity and the thermodynamics of the binding interaction. To the best of our knowledge, this work is the first to explore the role of Mg^{2+} in modifying the Ca^{2+} affinity of cTnC mutations linked to HCM. Our results indicate a physiologically significant role for cellular Mg^{2+} both at baseline and when elevated on modifying the Ca^{2+} binding properties of cTnC and the subsequent conformational changes which precede cardiac contraction.

Abbreviations
BME, β-mercaptoethanol; cTn, Cardiac troponin; cTnC, Cardiac troponin C; DCM, Dilated cCardiomyopathy; DTT, Dithiothreitol; EC, Excitation-contraction; HCM, Hypertrophic cCardiomyopathy; IPTG, Isopropyl β-D-1-thiogalactopyranoside; ITC, Isothermal titration calorimetry; LB, Lysogeny Broth; MBAR, Multistate Bennett Acceptance Ratio; MD, Molecular Dynamics; N, Molar ratio; N-cTnC, N-terminal domain of cardiac troponin C; NMR, Nuclear Magnetic Resonance; TF, Thin filament; TI, Thermodynamic Integration; TnIsw, cTnI switch peptide; TNNC1, cTnC gene.

Introduction

Cardiac troponin C (cTnC) is a dumbbell-shaped protein with 4 EF hand domains. High affinity structural sites III and IV in the C-terminal domain bind Ca^{2+} ($K_A \sim 10^7\ M^{-1}$) and Mg^{2+} ($K_A \sim 10^4\ M^{-1}$) to tether cTnC to the other components of the cardiac troponin (cTn) complex [1–3]. The N-terminal domain contains site I (which is dysfunctional in cardiac muscle) and site II which plays the critical regulatory role. Low affinity ($K_A \sim 10^5\ M^{-1}$) site II binds Ca^{2+} at elevated concentrations during systole (400–1000 nM) and is largely unbound during diastole (100 nM) [4]. cTnC is composed of nine α-helices: helices N, A, B, C and D in the N terminal-domain are linked through the flexible D-E linker to the C-domain which contains helices E, F, G and H. Binding of Ca^{2+} to site II acts as a conformational switch, causing helices N, A and D to move away from helices B and C to expose a hydrophobic cleft (Fig. 1). This region is then bound by the cTnI switch peptide (TnI_{sw}), causing further perturbation within the cTn complex and the rest of the thin filament (TF) to expose actin binding sites allowing for contact with myosin heads, ultimately resulting in force production [5–7].

Hypertrophic Cardiomyopathy (HCM) afflicts ~ 1 in 200 in the general population [8,9]. Over 1000 HCM-associated mutations have been found in a variety of sarcomeric proteins, of which over 100 are located in the cTn complex [10–13]. Despite a wide range of molecular precursors, the disease phenotype consistently entails hypertrophy, myocyte disarray and fibrosis [14,15]. This devastating disease often manifests as sudden cardiac arrest secondary to ventricular tachycardia/fibrillation and is the most common cause of sudden cardiac death in young athletes [16,17].

Hypertrophy has been posited to result from increased myofilament Ca^{2+} sensitivity which prolongs systole and shortens diastole [4]. Alternatively, hypertrophy may result from changes in maximum tension enacted by changes in tropomyosin displacement [18]. The role of cTnC as the Ca^{2+}-sensing component has made it a target of study with multiple HCM-associated mutations identified in the regulatory N-terminal domain [19,20]. While large-scale studies show a sparce number of pathogenic HCM-associated mutations in cTnC [21–24], this may be due to the central role this molecule plays in excitation-contraction (EC) coupling, whereby significant functional changes may be incompatible with physiological viability.

After potassium, Mg^{2+} is the second most abundant cellular cation with a total concentration of ~ 15–20 mM. Mg^{2+} is also tightly regulated through extensive buffering by cytosolic components such as ATP. A wide range of free Mg^{2+} concentrations between 0.2 and 3.5 mM have been reported in different systems with the majority of Mg^{2+} believed to exist in complex with ATP. The consensus is that the free $[Mg^{2+}]_i$ is ~ 0.5–1 mM making this cation approximately three orders of magnitude more abundant than systolic Ca^{2+} [25–27]. Short-term ischemia (~ 15 min) elevates free

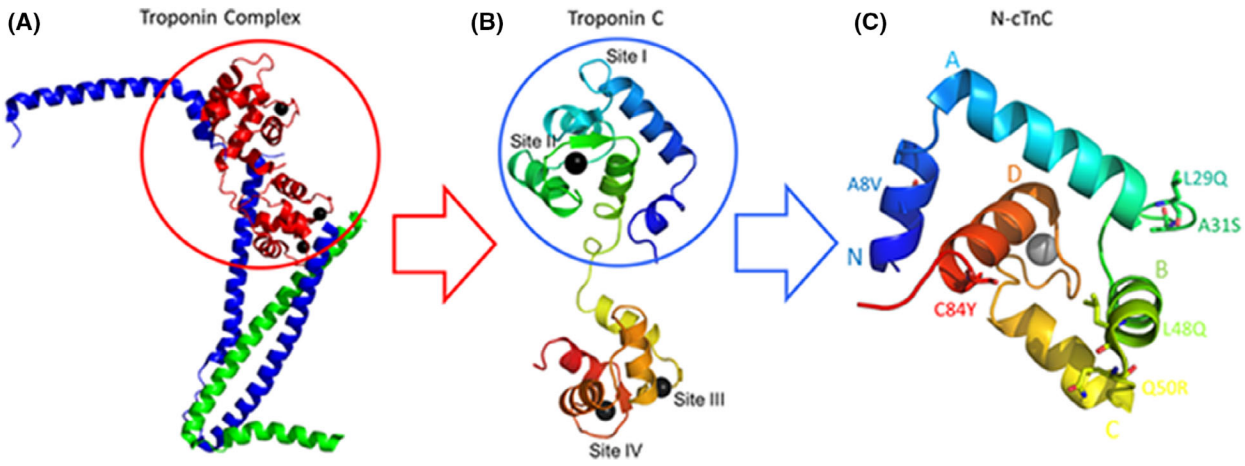

Fig. 1. N-cTnC within cTnC and the troponin complex. (A) the cTn complex is shown containing the core domain with some components excluded from the final protein structure to facilitate X-ray crystallography [108]. This complex includes the Ca^{2+} binding cTnC in red, the inhibitory cTnI in blue and the tropomyosin binding cTnT in green. Black spheres depict the bound cations that interact with sites III/IV in the C-terminal domain and site II in the N-terminal domain. (B) cTnC shown in rainbow colours with the N-terminal domain in blue and the C-terminal domain in red. (C) the N-domain of cTnC (N-cTnC) with six mutations of interest labelled. Helices N through D are labelled. For this figure, PYMOL was used to generate the cTnC structures.

Mg^{2+} up to 10-fold due primarily to a loss of $[ATP]_i$ [28,29]. Studies on isolated TnC [30–35], the cTn complex [30,32] and reconstituted fibres [32,36] have demonstrated that Mg^{2+} decreases the ability of Ca^{2+} to expose the hydrophobic cleft and cause subsequent structural changes in the rest of the cTn complex. Previous studies utilising physiological systems similarly demonstrated an inverse correlation between Ca^{2+} sensitivity of force production and availability of Mg^{2+} in skinned skeletal and cardiac fibres [37–39]. Three millimolar Mg^{2+} decreased the Ca^{2+} affinity in isolated cTnC [3] and skinned psoas muscles [40], but did not seem to cause structural changes in cTnC [3,41].

Equilibrium dialysis studies suggested that Mg^{2+} does not compete with Ca^{2+} for binding to the N-terminal cTnC and exclusively binds to the two C-terminal sites [42]. This notion has endured for decades. In the time since, however, several studies have shown through a number of different experimental techniques that the Mg^{2+} binding affinity of site II of skeletal and cardiac TnC is physiologically relevant [31,33,39,43–49]. The Mg^{2+} affinity of site II was estimated through fluorescence to have a K_A of $\sim 0.6 \times 10^3$ M^{-1} and through competition experiments, site II was posited to be 33–44% saturated with this cation at diastolic concentrations of Ca^{2+} [3]. More recent studies show that these results also hold in TnC variants of similar sequence from other species where Mg^{2+} binding affinity is an order of magnitude lower than Ca^{2+} [50]. Our recently published ITC and thermodynamic integration (TI) simulations corroborated and expanded upon these same findings [51].

A prevalent idea posits that contractile protein variants which destabilise the closed conformation of the protein prior to Ca^{2+} binding and/or those that favour the open, Ca^{2+}-bound state confer an increase in affinity [24]. Sequence variations outside the coordinating residues of the cTnC EF hands may induce alterations in Ca^{2+} affinity allosterically [52,53]. These changes in Ca^{2+} binding have previously been linked to HCM and Dilated Cardiomyopathy (DCM)-associated variants [41,54,55]. In contrast, variants outside the binding residues of each EF hand are not thought to allosterically modify Mg^{2+} binding [56–58]; therefore, the role of this cation in HCM is currently unclear. Here, we further explore the effects of Mg^{2+} on Ca^{2+} binding to the regulatory domain of cTnC and possible modifying affects on the previously listed series of HCM-associated variants.

In this study, we focus on the HCM-associated *TNNC1* variants A8V [59,60], L29Q [61], A31S [62] and C84Y [63,64], the engineered mutation L48Q [3] and the DCM-associated *TNNC1* variant Q50R [65] (Fig. 1). We have previously studied this series of mutations through Isothermal Titration Calorimetry (ITC) and Molecular Dynamics (MD) Simulations [55]. Our findings supported the notion that L48Q, Q50R and C84Y destabilise the closed-state of cTnC or stabilise the interaction with the TnI_{SW} in the open-state leading to an increase in Ca^{2+}-binding affinity. In contrast, A8V, L29Q and A31S were found to alter Ca^{2+}-coordination through a more subtle local structural perturbations [55].

We previously used ITC and thermodynamic integration simulations to show that physiological concentrations (1 mM) of free Mg^{2+} significantly reduce Ca^{2+}-binding to site II in both full-length and N-terminal cTnC [51]. It is important to establish whether cardiomyopathy associated variants affect binding of Ca^{2+}, Mg^{2+} or both. If the binding of these ions is affected unequally by a specific variant, then this could exacerbate or attenuate the effect when considering Ca^{2+} alone. This study compares Mg^{2+}-induced modifications in the Ca^{2+} binding properties of the regulatory site of cTnC with cardiomyopathy-associated *TNNC1* variants with Ca^{2+} and Mg^{2+} binding affinity shown to be different for each mutant. In particular, the affect of L48Q on the binding of these cations was significantly different from the WT, with Q50R and C84Y also showing some small, insignificant differences. These findings underline the importance of considering background Mg^{2+} levels which were studied through competition experiments. We show that affinity of the five HCM-associated variants (including L48Q which is engineered) and a single DCM-associated *TNNC1* variant for Mg^{2+} is higher than WT cTnC which is now established to have a physiological significant affinity for Mg^{2+}. Therefore, the presence of baseline Mg^{2+} may contribute to the dynamics which govern cardiac EC coupling. Further, higher than baseline concentrations of Mg^{2+} such as may occur during ischemia may accentuate the effects of inherited *TNNC1* variants and further exacerbate dysfunction in the diseased heart.

Results

Each N-cTnC construct was independently titrated by Ca^{2+} and Mg^{2+} in the apo-state. Each construct was also independently pre-incubated with 1 mM Mg^{2+} and 3 mM Mg^{2+} and titrated by Ca^{2+} to measure the relative binding affinity (Figs 2–7).

All studied *TNNC1* variants increased the binding affinity of both Ca^{2+} and Mg^{2+} relative to the WT construct (Fig. 2). The smallest increase was associated with A8V and the greatest with L48Q. In general, the

(A) Apo-state Ca^{2+}

N-cTnC	n	N	K_A *10^3 (M^{-1})	K_d (μM)	ΔH (kcal*mol^{-1})	T*ΔS (kcal*mol^{-1})	ΔG (kcal*mol^{-1})
WT	9	1.01 ± 0.01	64.48 ^{D} ± 3.09	15.79 ^{A} ± 0.74	3.58 ^{A} ± 0.07	10.14 ^{A} ± 0.08	-6.56 ^{A} ± 0.03
A8V	6	1.02 ± 0.01	75.57 ^{D} ± 1.29	13.25 ^{A} ± 0.23	3.43 ^{A} ± 0.04	10.09 ^{A} ± 0.04	-6.66 ^{A,B} ± 0.01
L29Q	5	1.04 ± 0.01	112.10 ^{C,D} ± 6.71	9.05 ^{B} ± 0.55	3.47 ^{A} ± 0.08	10.35 ^{A} ± 0.07	-6.89 ^{B} ± 0.03
A31S	6	1.00 ± 0.01	121.30 ^{C,D} ± 11.42	8.60 ^{B} ± 0.77	2.28 ^{B} ± 0.07	9.20 ^{B} ± 0.03	-6.93 ^{B} ± 0.06
L48Q	7	1.01 ± 0.01	394.71 ^{A} ± 7.26	2.54 ^{C} ± 0.05	-6.51 ^{E} ± 0.04	1.12 ^{E} ± 0.03	-7.63 ^{D} ± 0.01
Q50R	7	1.01 ± 0.01	232.86 ^{B,C} ± 24.14	4.61 ^{C} ± 0.52	1.43 ^{C} ± 0.04	8.74 ^{C} ± 0.04	-7.31 ^{C} ± 0.06
C84Y	7	1.00 ± 0.01	284.29 ^{A,B} ± 59.60	4.47 ^{C} ± 0.83	0.64 ^{D} ± 0.03	8.01 ^{D} ± 0.11	-7.37 ^{C} ± 0.12

(B) Apo-state Mg^{2+}

N-cTnC	n	N	K_A *10^3 (M^{-1})	K_d (μM)	ΔH (kcal*mol^{-1})	T*ΔS (kcal*mol^{-1})	ΔG (kcal*mol^{-1})
WT	7	1.00	1.43 ^{B} ± 0.07	711.08 ^{A} ± 32.67	2.50 $^{B, C}$ ± 0.18	6.79 ^{E} ± 0.17	-4.29 ^{A} ± 0.03
A8V	6	1.00	2.99 ^{B} ± 0.08	335.49 ^{B} ± 10.11	2.75 $^{B, C}$ ± 0.07	7.48 ^{D} ± 0.06	-4.74 ^{A} ± 0.02
L29Q	6	1.00	2.88 ^{B} ± 0.23	358.47 ^{B} ± 28.10	2.94 ^{B} ± 0.06	7.65 ^{D} ± 0.06	-4.70 ^{A} ± 0.05
A31S	6	1.00	4.24 ^{B} ± 0.35	245.69 ^{C} ± 24.04	2.72 $^{B, C}$ ± 0.08	7.65 $^{C, D}$ ± 0.10	-4.93 ^{A} ± 0.05
L48Q	7	1.00	175.70 ^{A} ± 23.50	6.29 ^{D} ± 0.84	3.91 ^{A} ± 0.23	11.04 ^{A} ± 0.19	-10.50 ^{B} ± 2.18
Q50R	7	1.00	22.03 ^{B} ± 0.99	45.97 ^{D} ± 2.14	2.27 ^{C} ± 0.10	8.18 $^{B, C}$ ± 0.09	-5.92 ^{A} ± 0.03
C84Y	8	1.00	29.89 ^{B} ± 3.53	36.52 ^{D} ± 3.92	2.29 ^{C} ± 0.06	8.37 ^{B} ± 0.05	-6.08 ^{A} ± 0.06

(C) +1mM Mg^{2+}

N-cTnC	n	N	K_A *10^3 (M^{-1})	K_d (μM)	ΔH (kcal*mol^{-1})	T*ΔS (kcal*mol^{-1})	ΔG (kcal*mol^{-1})
WT	8	1.00	41.45 $^{D, E}$ ± 2.98	25.13 ^{B} ± 2.06	2.36 ^{A} ± 0.11	8.65 ^{A} ± 0.09	-6.29 ^{B} ± 0.05
A8V	6	1.00	20.82 ^{E} ± 2.75	52.84 ^{A} ± 7.43	1.43 ^{B} ± 0.05	7.29 ^{B} ± 0.04	-5.86 ^{A} ± 0.08
L29Q	6	1.00	36.90 $^{D, E}$ ± 3.44	28.37 ^{B} ± 2.78	1.16 ^{B} ± 0.07	7.38 ^{B} ± 0.06	-6.22 ^{B} ± 0.06
A31S	8	1.00	169.00 ^{B} ± 17.68	6.36 ^{C} ± 0.62	-1.06 ^{C} ± 0.10	6.05 ^{C} ± 0.14	-7.11 ^{D} ± 0.06
L48Q	7	1.00	227.14 ^{A} ± 16.85	4.57 ^{C} ± 0.39	-7.46 ^{F} ± 0.14	-0.16 ^{F} ± 0.17	-7.30 ^{D} ± 0.05
Q50R	7	1.00	75.77 $^{C, D}$ ± 4.43	13.48 ^{C} ± 0.80	-4.67 ^{D} ± 0.11	1.98 ^{D} ± 0.14	-6.65 ^{C} ± 0.04
C84Y	7	1.00	86.69 ^{C} ± 2.14	11.58 ^{C} ± 0.29	-6.06 ^{E} ± 0.22	0.67 ^{E} ± 0.22	-6.74 ^{C} ± 0.01

(D) +3 mM Mg^{2+}

N-cTnC	n	N	K_A *10^3 (M^{-1})	K_d (μM)	ΔH (kcal*mol^{-1})	T*ΔS (kcal*mol^{-1})	ΔG (kcal*mol^{-1})
WT	8	1.00	22.6 ^{C} ± 2.01	46.37 ^{B} ± 3.40	1.63 ^{A} ± 0.07	7.55 ^{A} ± 0.06	-5.92 ^{B} ± 0.05
A8V	7	1.00	11.95 ^{C} ± 1.29	89.80 ^{A} ± 9.72	0.60 ^{B} ± 0.03	6.14 ^{B} ± 0.04	-5.55 ^{A} ± 0.06
L29Q	9	1.00	13.93 ^{C} ± 1.76	80.66 ^{A} ± 9.20	0.55 ^{B} ± 0.04	6.17 ^{B} ± 0.04	-5.62 ^{A} ± 0.07
A31S	7	1.00	62.84 ^{B} ± 6.32	16.80 ^{C} ± 1.49	-1.07 ^{C} ± 0.05	5.46 ^{C} ± 0.09	-6.53 $^{C, D}$ ± 0.06
L48Q	7	1.00	82.74 ^{A} ± 3.18	12.20 ^{C} ± 0.52	-6.67 ^{F} ± 0.17	0.04 ^{F} ± 0.19	-6.71 ^{D} ± 0.02
Q50R	7	1.00	49.34 ^{B} ± 2.17	20.50 ^{C} ± 0.89	-3.65 ^{D} ± 0.05	2.75 ^{D} ± 0.07	-6.40 ^{C} ± 0.02
C84Y	7	1.00	53.30 ^{B} ± 3.20	19.15 ^{C} ± 1.08	-4.72 ^{E} ± 0.09	1.73 ^{E} ± 0.12	-6.44 ^{C} ± 0.03

Fig. 2. The thermodynamic properties of the binding interactions with WT N-cTnC and each of the mutants are listed. The Ca^{2+} and Mg^{2+} experiments were the titration of each cation into apo-state protein while +1/3 mM Mg^{2+} indicates the concentration of Mg^{2+} in each sample cell prior to titration with Ca^{2+}. Each parameter is displayed the as mean ± SEM, with the exception of N which was fixed to 1.00 in the Mg^{2+} binding and pre-incubation experiments. ANOVA and subsequently Tukey's test were independently used to find difference between constructs for each parameter and titration. For each parameter, the mean of constructs not connected by the same letter indicates a statistically difference, $P < 0.05$.

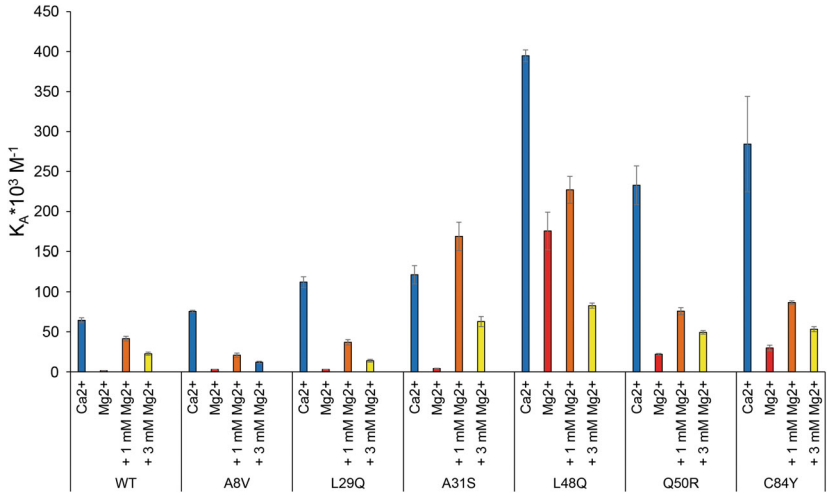

Fig. 3. Comparing the affinity for Ca^{2+}/Mg^{2+} in each titration condition between all N-cTnC constructs. The *x*-axis labels indicate the tiration conditions: 'Ca^{2+}' indicates the titration of this cation into apo-state protein, similarly 'Mg^{2+}' indicates titration into apo-state protein. '+1 mM Mg^{2+}' and '+3 mM Mg^{2+}' are the pre-incubation conditions for the construct into which Ca^{2+} was titrated; the affinity obtained is therefore seen in a sytem with both Ca^{2+} and Mg^{2+} present. SEM error bars are used to depict where significant differences exist in the mean values. Sample size for each condition was between 6–9 independent tirations. With the exception of L48Q, the highest affinity is seen in the Ca^{2+} titration and the lowest in the Mg^{2+} titrations. L48Q has the highest Mg^{2+} binding affinity by over an order of magnitude. Increasing Mg^{2+} from 0 to 1 to 3 mM lowered Ca^{2+} binding affinity in a graded manner. ANOVA and subsequent Tukey's *post-hoc* test indicate a number of differences in the mean K_A between the constructs and titration conditions. For the titrations Ca^{2+} in the apo-state, L48Q, C84Y and Q50R were significantly different from the WT. For the Mg^{2+} titrations in the apo-state, L48Q was significantly different from the WT. For pre-incubation with 1 mM Mg^{2+}, A31S, L48Q and C84Y were significantly different from the WT. For pre-incubations with 3 mM Mg^{2+}, L48Q was significantly different from the WT.

mutations adjacent to site II (L48Q, Q50R and C84Y) increased the affinity for each cation to a greater extent and altered the thermodynamic profile of the binding interaction more dramatically; the changes associated with the other mutants were more subtle.

The K_A associated with Mg^{2+} binding was orders of magnitude lower than that determined for Ca^{2+} binding for all constructs (Figs 2 and 3). The addition of 1 mM Mg^{2+} decreased both the amount of binding and affinity for Ca^{2+} at site II with 3 mM Mg^{2+} further accentuating the trend (Table 1).

Ca^{2+} binding

The interaction of Ca^{2+} with each construct was endothermic and entropically driven with the exception of L48Q in which the reaction was exothermic. Ca^{2+} bound to WT N-cTnC with a K_A of $64.5 \pm 3.1 \times 10^3$ M^{-1}, A8V had moderately higher binding affinity. Relative to WT N-cTnC, Ca^{2+} bound to each cTnC variant with higher affinity: L29Q and A31S (~ 2-fold), L48Q (~ 6-fold), Q50R (~ 3.5-fold) and C84Y (~ 4-fold). The ΔG reflects the ΔH and the ΔS and as such demonstrates that the most favourable interaction occurs in L48Q, then Q50R/C84Y, followed by the other mutants (Figs 2, 8, 9). These results are in agreement with our previously published work [51,55].

Mg^{2+} binding

The interaction of Mg^{2+} with WT N-cTnC was endothermic and entropically driven with a K_A of $1.4 \pm 0.1 \times 10^3$ M^{-1}; more than an order of magnitude lower binding affinity than seen with Ca^{2+}. Relative to the WT, Mg^{2+} binding to each mutant occurred with a

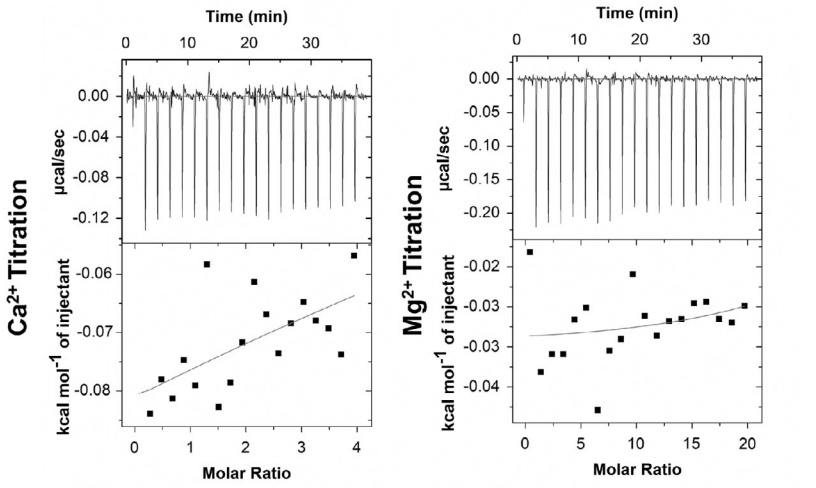

Fig. 4. Representative isotherms are presented to quantify the heat signal from the interaction with each of Ca^{2+} and Mg^{2+} with the buffer. N-values do not present any utility and are included for completeness. The buffer titrations involve only transient binding interactions such as hydrogen bonds and Van der Waals forces if indeed they are quantifiable, between the solutes and solvents; this system contains no protein and no true binding sites. The scale may be used as measure of the heat change in the system and a proxy to compare with the titrant into N-cTnC conditions. The values measured when a single binding site model was used to fit each titration are presented in the table.

Titrant	N	K_A *10^3 (M^{-1})	ΔH (kcal*mol^{-1})	ΔS (kcal*mol^{-1})
Ca^{2+}	1.19e3 ± 2.85e6	0.003 ± 7.06	-0.20 ± 5.00	0.432
Mg^{2+}	37.2 ± 115	3.74 ± 36.8	-0.03 ± 0.009	4.83

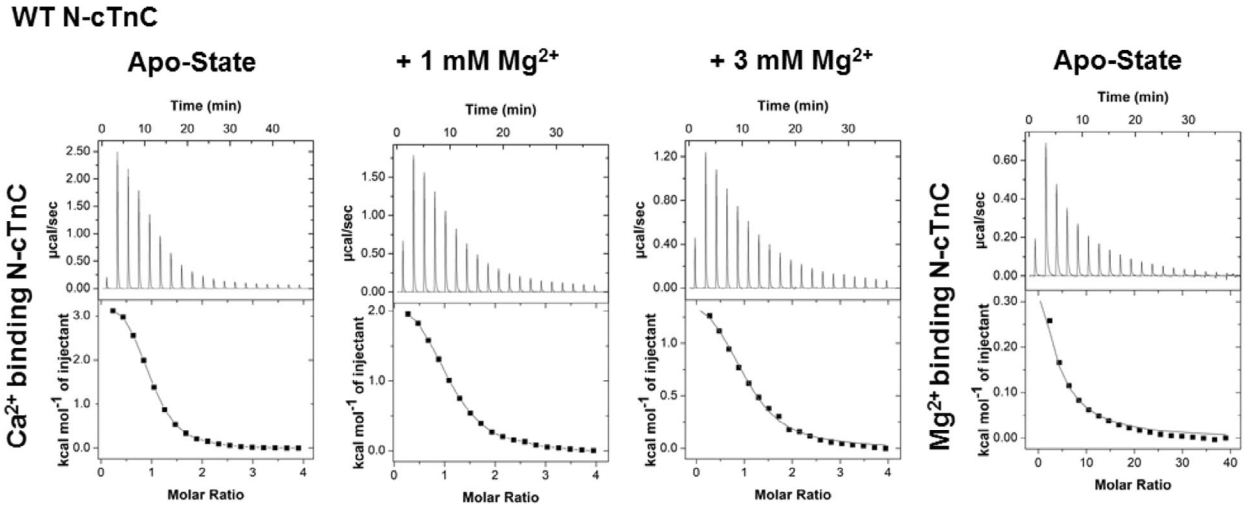

Fig. 5. Representative isotherms for each titration condition in the WT N-cTnC construct. From the left, the titration of Ca^{2+} into apo-state N-cTnC is shown, the next two panels show the titration of Ca^{2+} into 1 and 3 mM Mg^{2+} incubated WT N-cTnC. The right-most panel shows titration of Mg^{2+} into apo-state protein. Each titration is similarly endothermic with the scales indicating differences in absolute value of change in enthalpy.

similar energetic profile and with higher affinity: A8V and L29Q (~ 2-fold), A31S (~ 3-fold), L48Q (~ 120-fold), Q50R (~ 15-fold) and C84Y (~ 20-fold; Fig. 2). The ratio between Mg^{2+} and Ca^{2+} binding affinity was significantly greater than seen in the WT in L48Q and greater but not significantly so in Q50R and C84Y; these findings stress the need for competition experiments which allow for the study of Ca^{2+}-affinities in the presence of physiologically relevant Mg^{2+} concentrations (Fig. 10).

Ca^{2+} and Mg^{2+} competitive binding

Pre-incubation of WT N-cTnC with 1 mM Mg^{2+} lowered Ca^{2+}-binding affinity by 1.6-fold and 3 mM Mg^{2+} further accentuated the effect. Pre-incubation of A8V

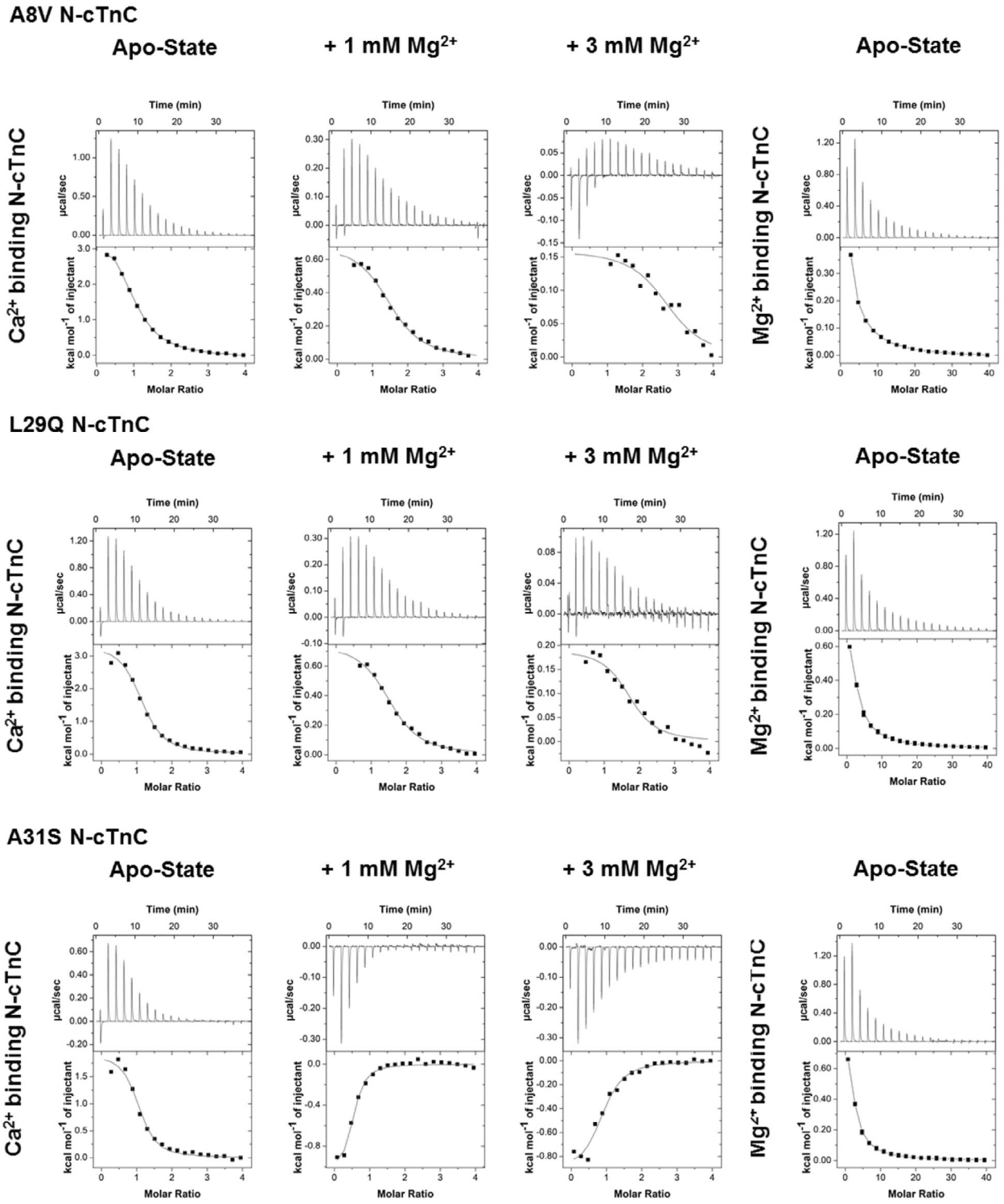

Fig. 6. Representative isotherms for each titration condition into A8V, L29Q and A31S N-cTnC. The three most N-terminal mutations are shown; A8V, L29Q and A31S from top to bottom. On the left panel, titration of Ca^{2+} into apo-state protein is illustrated with the next panels showing the titration of Ca^{2+} into 1 and 3 mM Mg^{2+} pre-incubated N-cTnC. The right-most panel shows the titration of Mg^{2+} into apo-state N-cTnC. The majority of titrations are characterised by an endothermic interaction with the exception of A31S, where pre-incubation with Mg^{2+} resulted in an exothermic interaction with Ca^{2+}.

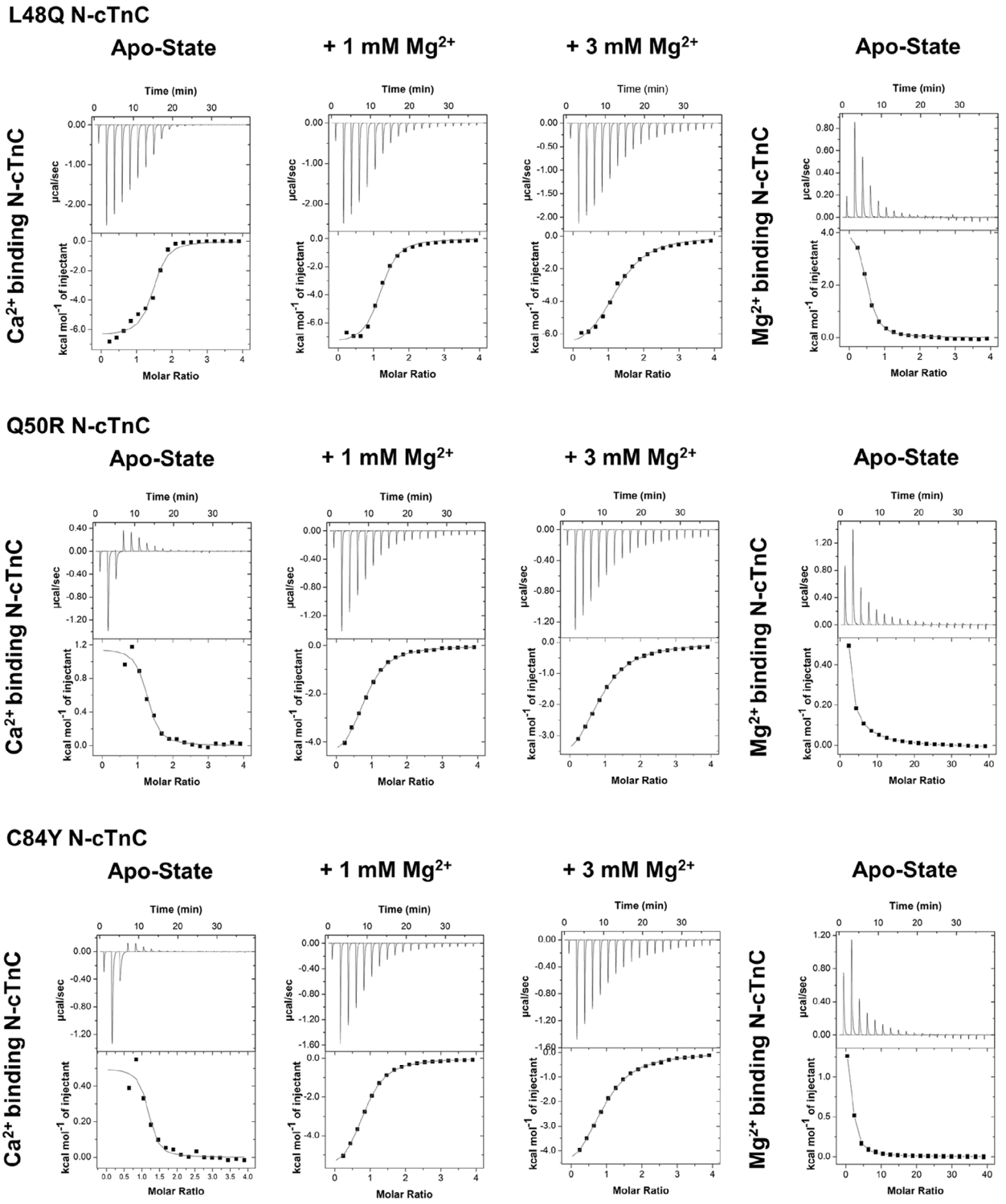

Fig. 7. Representative isotherms for each titration condition for L48Q, Q50R and C84Y N-cTnC. From top to bottom, isothermsfor L48Q, Q50R and C84Y are shown. On the left-most panel, titration of Ca^{2+} into apo-state protein is shown with the next panels showing the titration of Ca^{2+} into 1 and 3 mM Mg^{2+} pre-incubated N-cTnC. The right-most panel shows the titration of Mg^{2+} into apo-state N-cTnC. These three mutants caused the greatest deviation in thermodynamic properties from the WT titration conditions. The Ca^{2+} into apo-protein titration is endothermic for Q50R and C84Y but exothermic for L48Q. The Mg^{2+} into apo-protein titration is endothermic for all three mutants. The pre-incubation condition with both 1 and 3 mM Mg^{2+} resulted in an exothermic interaction with Ca^{2+}.

Table 1. Mg^{2+} restraint distances for thermodynamic integration.

	WT N-cTnC		L48Q		Q50R		C84Y	
Restraint 1	ASP67 CG Atom 1029	2.3 Å	ASP67 CG Atom 1027	2.3 Å	ASP67 CG Atom 1036	2.3 Å	ASP67 CG Atom 1029	2.3 Å
Restraint 2	SER69 OG Atom 1048	3.7 Å	SER69 OG Atom 1046	3.7 Å	SER69 OG Atom 1055	3.7 Å	SER69 OG Atom 1048	3.7 Å
Restraint 3	THR71 OG1 Atom 1067	4.5 Å	THR71 OG1 Atom 1065	4.5 Å	THR71 OG1 Atom 1074	4.5 Å	THR71 OG1 Atom 1067	4.5 Å

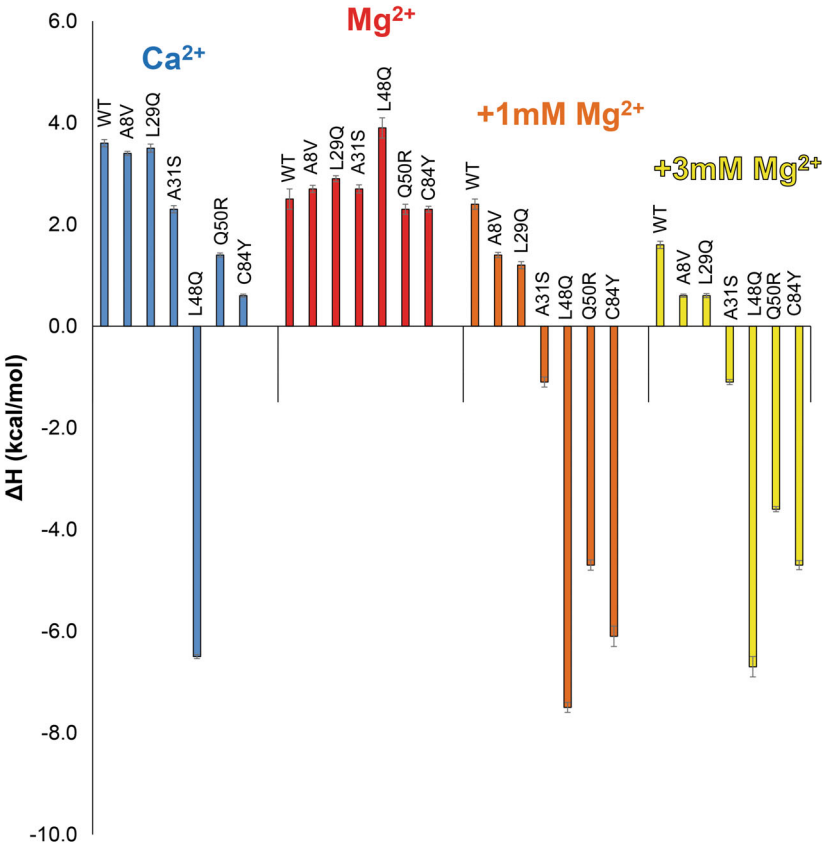

Fig. 8. Comparing the enthalpy for each Ca^{2+}/Mg^{2+} titration condition between all N-cTnC constructs. Ca^{2+} and Mg^{2+} experiements are titration of each cation into apo-state protein while +1/3 mM Mg^{2+} indicates the concentration of Mg^{2+} in each sample cell prior to titration with Ca^{2+}. SEM error bars are used to depict where significant differences exist in the mean values. Sample size for each condition was between six and nine independent tirations. ANOVA and subsequent Tukey's *post-hoc* test indicate a number of differences in the mean ΔH between the constructs and titration conditions. For the titrations with Ca^{2+} in the apo-state, A31S>Q50R>C84Y>>L48Q were significantly different from the WT. for the Mg^{2+} titrations in the apo-state, only L48Q was significantly different from the WT. for pre-incubation with 1 and 3 mM Mg^{2+}, all mutants were significantly different from the WT with A8V/L29Q most similar and L48Q most dissimilar from the WT.

with 1 and 3 mM Mg^{2+} reduced the Ca^{2+} affinity ~ 3 and 7-fold, respectively, and in L29Q the change was ~ 3 and 9-fold, respectively. One and 3 mM Mg^{2+} decreased the Ca^{2+}-affinity of L48Q by ~ 2 and 5-fold, respectively. Competition altered the reaction kinetics in A31S, Q50R and C84Y making each interaction exothermic and enthalpically driven. In A31S, 1 mM had a higher than apo-state affinity for Ca^{2+} (1.4-fold), yet 3 mM Mg^{2+} reduced Ca^{2+}-binding affinity (~ 2-fold). In both Q50R and C84Y N-cTnC, 1 and 3 mM Mg^{2+} lowered the Ca^{2+}-binding affinity 3- and 5-fold, respectively. L48Q, Q50R and C84Y affected Mg^{2+} and Ca^{2+}-binding to a different degrees, increasing Mg^{2+}-binding more than they increased Ca^{2+}-binding (Fig. 10).

Mg^{2+} binding affinities from thermodynamic integration (TI)

The binding affinity for each protein structure determined by Thermodynamic Integration was averaged over five independent runs and was -5.139 ± 2.308, -5.481 ± 0.719, -6.205 ± 2.112, -6.364 ± 1.372 kcal·mol^{-1}, respectively. The TI calculated Mg^{2+} binding affinities were in good agreement with the ITC data, except for L48Q N-cTnC. The ITC

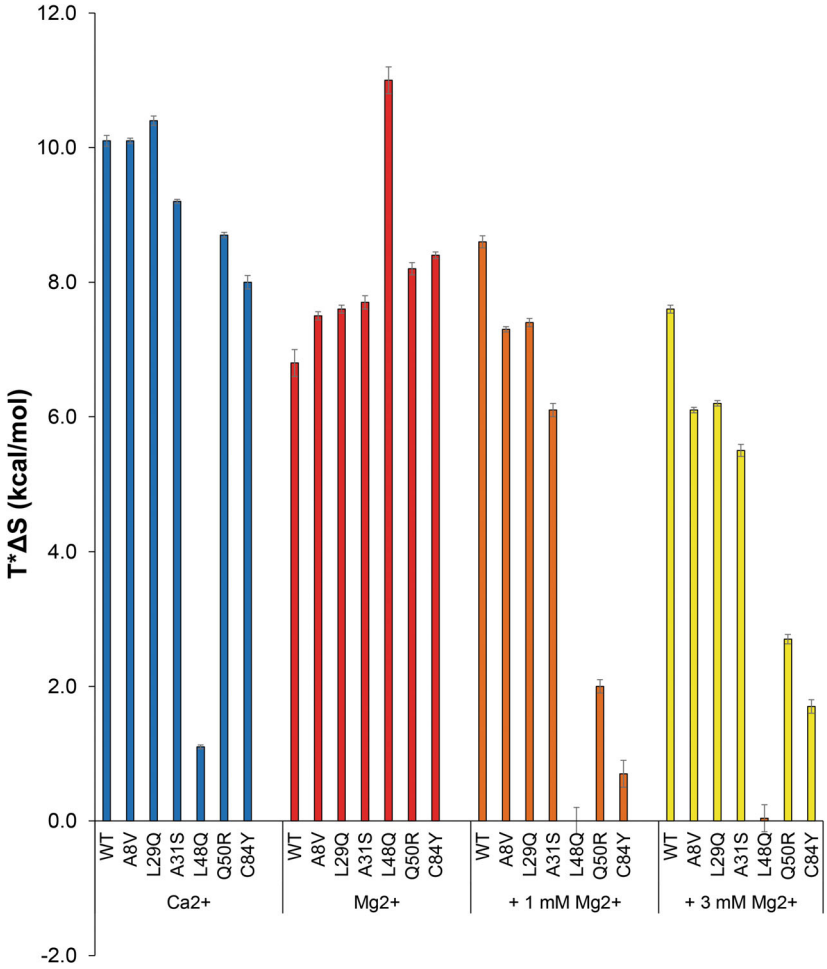

Fig. 9. Comparing the entropy for each Ca^{2+}/Mg^{2+} titration condition between all N-cTnC constructs. Ca^{2+} and Mg^{2+} experiements are titration of each cation into apo-state protein while +1/3 mM Mg^{2+} indicates the concentration of Mg^{2+} in each sample cell prior to titration with Ca^{2+}. SEM error bars are used to depict where significant differences exist in the mean values. Sample size for each condition was between six and nine independent tirations. ANOVA and subsequent Tukey's *post-hoc* test indicate a number of differences in the mean T*ΔS between the constructs and titration conditions. For the titrations with Ca^{2+} in the apo-state, A31S>Q50R>C84Y>>L48Q were significantly different from the WT. For the Mg^{2+} titrations in the apo-state, all conditions were significantly different and less than the WT. For pre-incubation with 1 and 3 mM Mg^{2+}, all titrations were significantly different and less than the WT.

data showed a much stronger increase in Mg^{2+} sensitivity for the L48Q N-cTnC. However, all mutated structures were shown to have increased Mg^{2+} sensitivity compared with WT cTnC. The $\Delta\Delta G_{Q50R}$ values were similar for TI and ITC (1.066 and 1.63 kcal·mol^{-1}, respectively). The $\Delta\Delta G_{C84Y}$ values also showed good agreement for TI and ITC (1.225 and 1.79 kcal·mol^{-1}, respectively; Table 2).

Discussion

The binding of Ca^{2+} to site II within the N-terminal domain of cTnC is the fundamental molecular precursor to a series of conformational changes that culminate in cross-bridge formation and force production. As such, changes in the sequence of this highly conserved protein often have grave consequences for the force production capabilities of the heart [66] and likely lead to cardiac remodelling. The six variants examined in this study all occur outside the EF hand binding regions and must allosterically alter Ca^{2+} affinity. Given the location of each mutation of interest and the desire to focus on changes in the binding interaction, we exclusively studied the N-terminal domain of cTnC. The mutations in question have also been studied at various levels of complexity by numerous groups, whose findings are in general agreement with our own [3,55,59,61–63,65]. In this study we found that the Ca^{2+} and Mg^{2+} binding affinity of the five HCM and a single DCM variant were variable and different from the WT. The Mg^{2+} affinities measured here, with the WT serving as a point of comparison, are physiologically significant and indicate a potential modulatory role for this cation in EC coupling.

The recently published Cryo-EM structure of the cardiac thin filament has shown that cardiomyopathy associated variants in troponin overwhelmingly occur in regions that interface with the actin-tropomyosin complex [67]. Variants which occur at a distance from these interfaces are still most likely to affect changes through altered interactions with other proteins of the

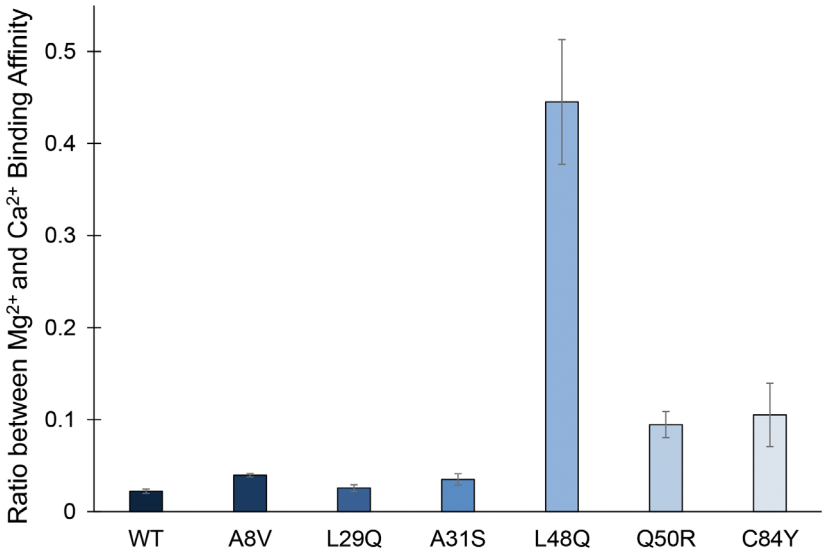

Fig. 10. Ratio between Mg^{2+} and Ca^{2+} binding affinity for each N-cTnC construct indicating the realtive change in affinity. Standard deviation error bars are also depicted to provide a measure of the confidence in each ratio. Sample size for each set of titrations for the constructs was between 6 and 9. A greater ratio indicates that the Mg^{2+}-binding affinity was greater in the construct relative to the baseline Ca^{2+}-binding affinity. ANOVA and subsequent Tukey's *post-hoc* test indicated that L48Q was significantly different from the other constructs, $P < 0.05$ with the other constructs not statistically distinguishable. The ratio is not equal to one in any of the constructs highlighting the importance of considering background cellular Mg^{2+} in these studies and stressing the importance of competition experiments.

Table 2. Mg^{2+} thermodynamic integration free energy of WT and mutant N-cTnC structures.

N-cTnC structure	ΔG_{TI}(kcal·mol^{-1}) ± std. dev.	$\Delta\Delta G_{TI}$
WT	−5.139 ± 2.308	
L48Q	−5.481 ± 0.719	−0.342
Q50R	−6.205 ± 2.112	−1.066
C84Y	−6.364 ± 1.372	−1.225

contractile complex [68]. These interactions may be affected by mutations occurring at the interface between proteins within the complex [69]. Thin filament loss-of-function variants are associated with HCM as they increase the Ca^{2+} sensitivity of contraction by decreasing the steric hinderance of myosin binding sites. In contrast, gain-of-function mutations in N-cTnC have a sensitising effect given that in the holo-state, this domain displaces the TnI_{SW} from actin, moves tropomyosin and unhinders myosin binding sites [21].

ITC directly measures the binding interaction and subsequent conformational change as an alternative to the introduction of naturally occurring fluorophores such as F27W [70] or synthetic fluorophores such as IAANS [41,71]. These reporters can be used to quantify the structural changes that proceed the binding interaction and thus, indirectly measure affinity. Fluorescence can also be used to report on the dissociation of Ca^{2+} from cTnC, the cTn complex or the TF by utilising chelators such as EDTA and rapid fluid changes through stopped flow experiments [53]. ITC has the sensitivity to detect minute enthalpic fluctuations which accompany these interactions, accurately detecting changes to within 0.1 μcal [72]. That is, not withstanding the inherent limitations associated with every experimental technique. For this assay a limitation results from the absence of other components of the cTn complex, particularly cTnI which plays a central role to the regulation of TF Ca^{2+} handling [41,67,73–75]; thus care must be taken when translating these findings to more complex systems.

The binding of Ca^{2+} to N-terminal cTnC is driven through a balance between the conformational strain resulting from the interaction and the energetics of exposing a hydrophobic cleft to the aqueous environment [76]. We posit that the changes in affinity seen in each *TNNC1* variant result from either the destabilisation of the apo-state protein or the stabilisation of the solvent exposed state [55]. We found that all of the HCM-associated cTnC variants studied had a more negative ΔG compared with the WT, consistent with our previously published MD Simulations [55]. Work by Bowman and Lindert [77] corroborates these findings and suggests a unifying theory that increased frequency of opening may result from the lowered energetic cost of exposing the N-terminal domain of

cTnC. The placement of more hydrophilic amino acids that destabilise hydrophobic packing in the closed state and stabilise the open, solvent-exposed state that follows may allow for this mechanism of action.

A8V was only moderately different from the WT, consistent with previous findings that suggest this mutation alters the interaction of cTnC with other TF proteins rather than altering the Ca^{2+} binding affinity directly [63,73]. The locus of valine near the interface with N-cTnI strengthens interaction with the switch peptide making this a distinct possibility [55,78]. Nuclear Magnetic Resonance (NMR) data suggest a slight increase in the opening frequency in the apo-state relative to the WT [59]. In our study, the binding affinity of this mutant for both Ca^{2+} and Mg^{2+} was higher than the WT. In pre-incubation experiments in which both cations were present, the A8V construct had lower than WT affinity for Ca^{2+} (Figs 2, 3, and 6).

L29Q nearly doubled the K_A for Ca^{2+} compared with WT, though the difference was not statistically significant. It also had greater than WT Mg^{2+} binding affinity but similar thermodynamic parameters and isotherm characteristics. Fluorescence (F27W) studies on isolated cTnC harbouring the L29Q mutation exhibited a nearly 2-fold increase in Ca^{2+} affinity [41]. A complex system containing the entire contractile apparatus with L29Q cTnC had similar to WT Ca^{2+} sensitivity [79]. This mutation also changes sensitivity of force generation in a length- and phosphorylation-dependent manner [52]. Changing a hydrophobic residue to one that is polar increases site II Ca^{2+} sensitivity [80,81]. Mechanistically, solvent exposure of an uncharged glutamine may facilitate a greater extent of opening than a hydrophobic leucine [55]. However, our previous work suggests that this variant has the highest closed probability among the seven constructs studied and lowers opening frequency [55]. In contrast, it has been shown through NMR that this mutation may cause a more open N-domain in the cTnC in both the apo- and holo-states [82]. L29Q may open in the holo-state with similar frequency as the WT and have similar energetic requirements as the WT for opening in both the apo- and holo-states [77]. Therefore, it is likely that the effects of this mutation in isolated N-cTnC are minimal and that changes are enacted through modification of the interaction with other cTn complex proteins [41].

The A31S *TNNC1* variant is the result of a change of a hydrophobic amino acid for an uncharged one within the site I EF hand. In skeletal tissue, there is a great deal of cooperativity between binding to the two N-terminal sites of TnC [83,84]. This mutant was found to have a greater K_A for both Ca^{2+} and Mg^{2+} compared with the WT and significantly higher affinity for Ca^{2+} in both pre-incubation conditions. A31S was found through MD simulations to sample a greater number of interhelical angles and to have a lower average angle between helices A and B [55]. Interestingly, pre-incubation with Mg^{2+} completely changed the reaction dynamics (Fig. 6). ΔH reflects the strength of hydrogen bonds, van der Waals interactions and electrostatic forces between the titrant and the target ligand. Optimal placement of hydrogen bond donors and acceptors balances de-solvation of polar groups to contribute to the enthalpy change [85]. The significant change in enthalpy suggests alteration of the number of bonds formed by the side chains of binding site residues or those exposed to the environment following the conformational change. This mutation may stabilise binding site I between helices A and B through formation of an additional hydrogen bond causing local changes that minimally alter global structure [62].

L48Q significantly altered affinity and thermodynamics of the binding interactions studied. The combination of high Ca^{2+} and Mg^{2+} affinity resulted in the highest observed K_A in both competition conditions. This is not unexpected, as the mutant is located within the BC helical bundle and was strategically engineered to increase the Ca^{2+} sensitivity of force production [3]. Our previously published MD simulations suggest that the absence of a hydrophobic residue disrupts hydrophobic packing in the AB domain. We also reported that the L48Q mutant opens more frequently than the other constructs [55,77]. The changes in ΔH are likely due in part to the presence of an additional hydrogen bonds resulting from the introduction of a polar amino acid in a key domain of cTnC. *In vivo*, this would increase the opportunities for interaction with the TnI_{sw} [17,86,87]. Tikunova and Davis [3] originally suggested that despite a shift towards the Ca^{2+}-bound state, resulting from a reduction in hydrophobic contact between helices NAD and BC, the solvent exposure of the N-domain is minimised by numerous side chain contacts. Their hypothesis regarding the disruption of hydrophobic interactions and minimisation of exposure to the surrounding solvent is reconcilable with our findings and explains the much lower ΔS associated with this set of titrations.

Q50R is a relatively recently identified mutation that has yet to be fully explored. This mutant replaces a polar side chain with one that is bulky and charged. Given the results in L48Q and the vicinity of these residues, it is conceivable that the packing of helices NAD and BC is also disrupted by this mutant. This

mutant had a much higher affinity than WT for both Ca^{2+} and Mg^{2+}. Similar to L48Q, the interaction with Ca^{2+} was exothermic in the pre-incubation condition. Our previous work suggests that Q50R is more frequently open than the WT cTnC [55]. The reduced entropic cost of exposing a more charged residue to the aqueous environment may explain the decreased ΔS of the system, yet the adjacent residues would also be exposed to variable degrees in this mutant. Further, the energetic cost of opening the hydrophobic patch is increased in this mutant in comparison to the WT protein that has a less stable closed conformation [77].

C84Y places a bulky hydrophobic side chain in the region immediately preceding the flexible DE linker that is bound and stabilised in the open state by the TnI_{SW}. This bulky tyrosine may act as a wedge to reduce interaction with the TnI_{SW} and thus increase the Ca^{2+} sensitivity of force development in skinned fibres [63,73]. C84Y was thermodynamically similar across all titrations with Q50R; given the location of these mutants, this does not necessarily suggest a similar mode of action. Interestingly, however, our MD Simulations previously showed that a hydrophobic interaction between C84 and Q50 may be disrupted by this tyrosine. The bulky tyrosine in helix D may reduce the entropic cost of opening associated with the binding interaction, this is consistent with the observed, lower than WT ΔS values in C84Y N-cTnC [55].

The calculated Mg^{2+} binding affinity results using TI were in good agreement with the ITC values. We observed increased ion sensitisation for all mutant N-cTnC structures. In particular the $\Delta\Delta G_{TI}$values for Q50R and C84Y mutations aligned very well with the experimental data. The absolute binding affinities calculated for WT, Q50R and C84Y were overestimated compared with the ITC values by less than 1 kcal·mol^{-1}. Parameterisation of cations, especially Mg^{2+}, in simulating biological systems has proven to be difficult [88,89]. This could offer a potential explanation for the overestimation and relatively high standard deviations observed in the averaged absolute binding affinities. Another source of discrepancy between the *in silico* and ITC results arises from the fact that there is no PDB structure of Mg^{2+} bound to site II of N-cTnC. In order to create the starting structure for TI simulations, the PDB 1AP4 served as the base model, and Mg^{2+} was substituted in place of the Ca^{2+} ion. If crystal structures of Mg^{2+}-bound WT N-cTnC and mutants were to exist, the use of these structures could potentially improve the TI results. TI of the L48Q mutant did not produce nearly as strong an increased Mg^{2+} sensitisation as observed in the ITC data. We speculate that this could possibly be attributed to large conformational changes that were unable to be captured using TI. The timescale of the TI simulations was only 5 ns, which was insufficient to properly sample any large protein conformational changes.

Our data clearly demonstrate that each of the N-cTnC variants, including the WT, responded significantly but variably to the presence of Mg^{2+}. Except for A31S, each mutant site II has a significantly lower Ca^{2+} binding affinity in the presence of 1 mM Mg^{2+}. The degree of desensitisation is best described as A8V>L29Q>Q50R>C84Y>L48Q. Given these observations, it is possible that Mg^{2+} binding dampens the presupposed sensitising effect of HCM-associated mutations (Chang and Potter 2005);[109] at the very least, the role of background Mg^{2+} in modifying Ca^{2+} sensitivity of force production cannot be ignored.

Given the high concentration of free Mg^{2+} in the cytosol and its similarities as a divalent cation and the small difference in atomic radius in comparison to Ca^{2+}, this ion is a candidate for binding to site II of cTnC. A polar serine at residue 69 and a negatively charged glutamic acid at residue 76 in the EF hand binding site II of N-cTnC create a domain that is amicable to Mg^{2+} binding [90,91]. Despite previous work in this field, the central dogma in the literature is largely dismissive of the possibility that physiologically relevant concentrations of Mg^{2+} bind to site II. We previously explored Mg^{2+} binding to site II in full length and N-terminal cTnC and established competition with Ca^{2+} at physiological concentrations of each cation in the cell [51]. In this work, we explore the hypothesis that Ca^{2+} and Mg^{2+} compete, where affinity for each cation is allosterically modified by single amino acid changes outside the binding domain.

Tikunova and Davis [3] have shown that Mg^{2+}, unlike Ca^{2+}, does not cause a structural change in the troponin complex upon binding but does significantly alter the affinity of cTnC for Ca^{2+} ; with 3 mM Mg^{2+} causing a more than 3-fold reduction in Ca^{2+} binding affinity. Moreover, Mg^{2+} reverses the fluorescence change of Ca^{2+} saturated cTnC; that is to say, their data support the concept that 3 mM Mg^{2+} competes for binding to site II.

The molecular mechanisms which underpin the role of cellular Mg^{2+} in cardiac contractility are yet to be fully understood and require further exploration. We measured a 47-fold difference in the affinity of WT N-cTnC for Ca^{2+} ($64.48 \pm 3.09 \times 10^3$ M^{-1}) in comparison to Mg^{2+} ($1.43 \pm 0.07 \times 10^3$ M^{-1}). However, the free Mg^{2+} concentration is 3 orders of magnitude more abundant in the cytosol at systole than Ca^{2+} (1 vs. 1000 {M); [92,93] and may compete for binding to site

II in addition to the structural sites III and IV [51]. Mg^{2+} deficiency has been linked to cardiac disease including arrhythmias, hypertension and congestive heart failure [94–97]. It is possible that Mg^{2+} modulates the role of Ca^{2+} and alters activation of contractile pathways that are governed by this messenger.

Less than 15 min of ischemia can substantially decrease $[ATP]_i$ resulting in a three-fold increase in free $[Mg^{2+}]$ [98]. This elevated Mg^{2+} may compete with Ca^{2+} for binding to cytosolic buffers such as cTnC. Overall, our study suggests that the effect of cellular Mg^{2+} on the Ca^{2+} binding properties of site II within N-cTnC is not negligible. This effect may be even more pronounced in HCM- and DCM-mutant N-cTnC, where both cytosolic concentrations of free Mg^{2+} (1 mM) and elevated Mg^{2+} that may accompany energy depleted states (3 mM) causing a more significant reduction in affinity compared with the WT through alterations in structural dynamics and the energetic landscape of each interaction.

Conclusions

The interaction of Ca^{2+} with mutant N-cTnCs occurred with higher than WT affinities, with the highest affinity seen in the L48Q mutant. In general, A31S, L48Q, Q50R and C84Y had the highest affinities for both Ca^{2+} and Mg^{2+}. Thermodynamic, structural and simulation work by our group and others suggests a common mechanism whereby mutants destabilise hydrophobic interactions between helices NAD and BC to elevate binding affinity.

We found that the affinity for Mg^{2+} ($\sim 1.5 \times 10^3$ M^{-1}) was at least an order of magnitude lower than that seen for Ca^{2+} ($\sim 60 \times 10^3$ M^{-1}). The change in affinity observed when comparing the Mg^{2+} pre-incubated N-cTnC and apo-state protein was variable in each mutant and significantly different from the WT. Moreover, 1 and 3 mM Mg^{2+} caused a graded decrease in the amount of binding and affinity for Ca^{2+}. In contrast to Ca^{2+}, cellular Mg^{2+} does not cause a conformational change upon binding to site II of cTnC and thus cannot initiate contraction. However, Mg^{2+} has been shown, both here and in numerous previous studies, to interact with the same N-terminal locus. Cellular Mg^{2+} may be altered in disease states; for example, it may be elevated in ischemic stress or decreased in hyperparathyroidism. Moreover, Mg^{2+}-binding to cTnC may alter the already skewed Ca^{2+}-cTnC binding interaction which exists in diseases such as HCM or DCM, further affecting significant changes in cardiomyocyte EC coupling.

Materials and methods

Construct preparations

Recombinant proteins were expressed and purified as described previously [99]. In brief, the human cTnC gene (*TNNC1*) within the pET-21a(+) vector was ordered from Novagen and the Phusion site-directed mutagenesis kit (Thermo) was used to introduce a stop codon at residue 90, followed by single base pair changes to introduce all six variants of interest (A8V, L29Q, A31S, L48Q, Q50R and C84Y) on separate N-terminal constructs ($cTnC_{1–89}$). Mutagenesis was carried out with preliminary steps using the DH5α *Escherichia coli* strain to house the plasmids. Following the mutagenesis and confirmation by sequencing, the constructs were transformed into the BL21(DE3) expression strain and stored as glycerol stocks.

Protein expression

Hundred millilitre of Lysogeny Broth (LB) supplemented with 50 μg·mL^{-1} of Ampicillin and a stab of the glycerol stock was grown overnight at 37 °C for 16–20 h with shaking at 225–250 r.p.m. One-litre flasks of LB were induced with 1–5% of the overnight culture and supplemented with the same concentration of antibiotic and grown under the same conditions for ~ 3 h (until the OD_{600} was between 0.8–1.0). The culture was then supplemented with 1 mM isopropyl β-D-1-thiogalactopyranoside (IPTG) and grown for a further 3–4 h. Cells were then harvested by centrifugation and resuspended in the Lysis Buffer (50 mM Tris-Cl and 100 mM NaCl at pH 8.0). The suspended pellet was stored at −80 °C until purification.

Protein purification

The pellet was thawed and sonicated at ~ 80% amplitude in 30 s intervals for a total time of 3–4 min with each intermittent period spent on ice. The cells were then spun two times, for 15 min each at 30 000 × ***g*** and the supernatant kept and the pellet discarded. The supernatant was filtered as needed and applied to a 15 mL fast-flow DEAE or Q Sepharose column (GE Healthcare, Chicago, IL, USA), pre-equilibrated with Buffer A (in mM 50 tris-Cl, 100 NaCl and 1 dithiothreitol (DTT) at pH 8.0). Buffer B (Buffer A + 0.55 M NaCl) was applied over a 180 mL protocol, in which the concentration was ramped up from 0 to 100% to elute the proteins of interest. Fractions containing the N-terminal cTnC construct were identified by SDS/PAGE and pooled. An Amicon centrifugal concentrator (Millipore, Burlington, MA, USA) with a 3 KDa cut-off was used to concentrate the pooled samples to a volume of 3–5 mL. The pooled samples were then applied to a HiPrep 26/60 Sephacryl S-100 column (GE Healthcare) equilibrated with

Buffer A. The fractions were again analysed by SDS/PAGE and those containing the protein of interest, free of contaminants were pooled, concentrated and stored at −80 °C.

ITC protocol

The protein was dialysed against three exchanges of 2 L for at least 6 h each with ITC Buffer 1 containing (in mM) 50 HEPES, 150 KCl, 2 EDTA and 15 β-mercaptoethanol (BME) at pH 7.2. ITC Buffer 2 was identical to the first but did not contain EDTA; this was the second buffer used for equilibration and was used after the first to remove the EDTA contained in Buffer 1. ITC Buffer 3 was identical to the second but contained significantly reduced BME (2 mM). Buffer 3 was used to dilute the protein and Ca^{2+}/Mg^{2+} prior to ITC experiments. A Nanodrop instrument was used to gain a preliminary measure of the protein concentration using an extinction coefficient of 1490 $M^{-1}{\cdot}cm^{-1}$ and a molecular weight of 10.4 kDa. An initial ITC run was used to determine the molar ratio (N). Given that the concentration of the titrant is known and the number of cation binding sites in N-cTnC is 1, the concentration of folded, functional protein was determined and adjusted in subsequent runs to give an N of 1.0.

The protein was diluted in the final dialysis buffer to a final concentration of 100 μM. The titrating solutions were prepared from 1.00 M Ca^{2+} and Mg^{2+} stocks (Sigma) by serial dilution in the final dialysis buffer. For the apo-state experiments, 2 mM Ca^{2+} and 20 mM Mg^{2+} were titrated into 100 μM N-cTnC with the exception of the L48Q in which 2 mM Mg^{2+} was used. For competition experiments, the apo-state construct was pre-incubated with Mg^{2+} to a final concentration of 1 or 3 mM Mg^{2+} prior to titration with 2 mM Ca^{2+}. Titrant into buffer blank experiments was carried out to gauge the impact of these experiments and indicate minimal heat change resulting from the interactions (Fig. S1). For all experiments, 19 titrations, 60 s apart, were performed with the first being 0.8 μL and each subsequent injection 2 μL. The cell contents were mixed at 750 r.p.m. throughout the titration. All titrations were carried out at 25 °C.

Data processing and statistical analysis

Data were imported and analysed in ORIGIN 8.0 software for Microcal ITC_{200} (Northampton, MA, USA). After saturation, the final 2–3 data points were averaged, the heat was subtracted from all injections as a control for heat of dilution and non-specific interactions. Least-squares regression was used to fit each titration after the first (dummy) injection was removed with minimisation of chi-square and visual evaluation used to determine the goodness-of-fit for a single binding site model. Following establishment of the protein concentration based on the obtained N value for each apo-state Ca^{2+} titration for each construct, the same dilution of protein was used for each other titration and the N-value fixed to 1.00 to facilitate data fitting. The various thermodynamic parameters were averaged and reported as mean ± SEM. The difference between the means was compared using a one-way ANOVA. This was followed by Tukey's *post-hoc* test to determine where significant ($P < 0.05$) differences existed (Fig. 2).

Thermodynamic integration (TI)

The structure of the N-terminal domain of cardiac troponin C (N-cTnC) was obtained from PDB:1AP4 [100], this structure contained N-cTnC with a single Ca^{2+} ion bound. Since there was no model of Mg^{2+} bound N-cTnC in the protein databank, we made use of the Mg^{2+} substituted structure as outlined in our previous work [51]. The model was then solvated using the tLeap module of AMBER 16 [101] in a 12 Å TIP3P water box and neutralised with Na^{+} ions; the forcefield used to describe the protein was ff14SB [102]. In order to complete the thermodynamic cycle, a system containing the Mg^{2+} ion was prepared using the tLeap module, referencing the $\Delta G_{solvation}$ optimised Mg^{2+} parameters from Li et al. [103], and solvated in a 12 Å TIP3P water box. Simulations were conducted under NPT conditions using the Berendsen barostat and periodic boundary conditions. The system was minimised for 2000 cycles and heated to 300 K using the Langevin thermostat over 500 ps prior to the 5 ns production with a time step of 2 fs. The SHAKE algorithm was employed to constrain all bonds involving hydrogen atoms, and the Particle Mesh Ewald method [104] was utilised to calculate electrostatic interactions of long distances with a cut-off of 10 Å.

The alchemical thermodynamic cycle used for ligand binding has been detailed previously by Leelananda and Lindert [105]. In this implementation of TI, the method consisted of three steps for ligand (Mg^{2+}) in protein: (a) introduction of harmonic distance restraints; (b) removal of electrostatic interactions and (c) removal of van der Waals forces. TI consisted of two steps for the ligand in water system: removal of electrostatic interactions and removal of van der Waals forces. The coupling parameter (λ) increased incrementally by 0.1 from 0.0 to 1.0 for each transitional step of the thermodynamic cycle. During each simulation $dV/d\lambda$ values were collected every 2 ps resulting in 5000 data points per transitional step of λ for further analysis. The Multistate Bennett Acceptance Ratio (MBAR) [106] was used to calculate the relative free energies of the simulations across all values of λ. Free energy (ΔG) corrections were made due to the introduction of the distance restraints and to correct for the charge of the system as described previously [51]. For each system, five independent runs were performed, and the results averaged. The specific distance restraints for all protein structures are shown in Table 1.

The cTnC variants (L48Q, Q50R, C84Y) were constructed using the protein mutagenesis tool in PYMOL [102,107] and the Mg^{2+} substituted representative model of N-cTnC serving as the base model. TI simulations were performed on the mutant structure as detailed above for the wild type.

Acknowledgements

The authors gratefully acknowledge the generous support from the Canadian Institutes of Health Research which funded this research project.

Conflict of interest

The authors declare no conflict of interest.

Author contributions

Preliminary Experiments – KR, ERH. Experimental Design - KR, ERH, OH-G, YAL, AMS, FVP, RJS, SL, GFT. Data Collection – KR, ERH. Data Analysis – KR, ERH, SL. Manuscript Preparation – KR, ERH, FVP, SL, GFT. Manuscript Review – KR, ERH, AMS, FVP, RJS, SL, GFT.

Data availability statement

Data is available upon request.

Peer review

The peer review history for this article is available at https://publons.com/publon/10.1111/febs.16578.

References

1 Potter JD, Gergely J. The calcium and magnesium binding sites on troponin and their role in the regulation of myofibrillar adenosine triphosphatase. *J Biol Chem*. 1975;**250**:4628–33.
2 Sturtevant JM. Heat capacity and entropy changes in processes involving proteins. *Proc Natl Acad Sci USA*. 1977;**74**:2236–40.
3 Tikunova SB, Davis JP. Designing calcium-sensitizing mutations in the regulatory domain of cardiac troponin C. *J Biol Chem*. 2004;**279**:35341–52.
4 Bers DM. Calcium fluxes involved in control of cardiac myocyte contraction. *Circ Res*. 2000;**87**:275–81.
5 Sia SK, Li MX, Spyracopoulos L, Gagné SM, Liu W, Putkey JA, et al. Structure of cardiac muscle troponin C unexpectedly reveals a closed regulatory domain. *J Biol Chem*. 1997;**272**:18216–21.
6 Kirschenlohr HL, Grace AA, Vandenberg JI, Metcalfe JC, Smith GA. Estimation of systolic and diastolic free intracellular Ca^{2+} by titration of Ca^{2+} buffering in the ferret heart. *Biochem J*. 2000;**346**(Pt 2):385–91.
7 Tardiff JC. Thin filament mutations: developing an integrative approach to a complex disorder. *Circ Res*. 2011;**108**:765–82.
8 Maron BJ, Gardin JM, Flack JM, Gidding SS, Kurosaki TT, Bild DE. Prevalence of hypertrophic cardiomyopathy in a general population of young adults echocardiographic analysis of 4111 subjects in the CARDIA study. *Circulation*. 1995;**92**:785–9.
9 Semsarian C, Ingles J, Maron MS, Maron BJ. New perspectives on the prevalence of hypertrophic cardiomyopathy. *J Am Coll Cardiol*. 2015;**65**:1249–54.
10 Seidman CE, Seidman JG. Identifying sarcomere gene mutations in hypertrophic cardiomyopathy: a personal history. *Circ Res*. 2011;**108**:743–50.
11 Ashrafian H, Watkins H. Reviews of translational medicine and genomics in cardiovascular disease: new disease taxonomy and therapeutic implications: cardiomyopathies: therapeutics based on molecular phenotype. *J Am Coll Cardiol*. 2007;**49**:1251–64.
12 Harada K, Morimoto S. Inherited cardiomyopathies as a troponin disease. *Jpn J Physiol*. 2004;**54**:307–18.
13 Reinoso TR, Landim-Vieira M, Shi Y, Johnston JR, Chase PB, Parvatiyar MS, et al. A comprehensive guide to genetic variants and post-translational modifications of cardiac troponin C. *J Muscle Res Cell Motil*. 2021;**42**:323–42.
14 Elliott P, McKenna WJ. Hypertrophic cardiomyopathy. *Lancet*. 2004;**363**:1881–91.
15 Goldspink PH, Warren CM, Kitajewski J, Wolska BM, Solaro RJ. A perspective on personalized therapies in hypertrophic cardiomyopathy. *J Cardiovasc Pharmacol*. 2021;**77**:317–22.
16 Maron BJ, Shirani J, Poliac LC, Mathenge R, Roberts WC, Mueller FO. Sudden death in young competitive athletes: clinical, demographic, and pathological profiles. *JAMA*. 1996;**276**:199–204.
17 Davis J, Davis LC, Correll RN, Makarewich CA, Schwanekamp JA, Moussavi-Harami F, et al. A tension-based model distinguishes hypertrophic versus dilated cardiomyopathy. *Cell*. 2016;**165**:1147–59.
18 Matsuo T, Kono F, Fujiwara S. Effects of the cardiomyopathy-causing E244D mutation of troponin T on the structures of cardiac thin filaments studied by small-angle X-ray scattering. *J Struct Biol*. 2019;**205**:196–205.
19 Katrukha I. Human cardiac troponin complex. Structure and functions. *Biochem Mosc*. 2013;**78**:1447–65.
20 Kalyva A, Parthenakis FI, Marketou ME, Kontaraki JE, Vardas PE. Biochemical characterisation of troponin C mutations causing hypertrophic and dilated cardiomyopathies. *J Muscle Res Cell Motil*. 2014;**35**:161–78.

21 Tobacman LS, Cammarato A. Cardiomyopathic troponin mutations predominantly occur at its interface with Actin and tropomyosin. *J Gen Physiol*. 2021;**153**:e202012815.

22 Alfares AA, Kelly MA. Results of clinical genetic testing of 2912 probands with hypertrophic cardiomyopathy: expanded panels offer limited additional sensitivity. *Genet Med*. 2015;**17**:880–8.

23 Tadros HJ, Life CS, Garcia G, Pirozzi E, Jones EG, Datta S, et al. Meta-analysis of cardiomyopathy-associated variants in troponin genes identifies loci and intragenic hot spots that are associated with worse clinical outcomes. *J Mol Cell Cardiol*. 2020;**142**:118–25.

24 Willott RH, Gomes AV, Chang AN, Parvatiyar MS, Pinto JR, Potter JD. Mutations in troponin that cause HCM, DCM AND RCM: what can we learn about thin filament function? *J Mol Cell Cardiol*. 2010;**48**:882–92.

25 Dai LJ, Friedman PA, Quamme GA. Phosphate depletion diminishes Mg^{2+} uptake in mouse distal convoluted tubule cells. *Kidney Int*. 1997;**51**:1710–8.

26 Romani A, Scarpa A. Regulation of cell magnesium. *Arch Biochem Biophys*. 1992;**298**:1–12.

27 Maguire ME. Magnesium transporters: properties, regulation and structure. *Front Biosci*. 2006;**11**:3149–63.

28 Krause SM, Rozanski D. Effects of an increase in intracellular free [Mg^{2+}] after myocardial stunning on sarcoplasmic reticulum Ca^{2+} transport. *Circulation*. 1991;**84**:1378–83.

29 Kirkels J, Van Echteld C, Ruigrok T. Intracellular magnesium during myocardial ischemia and reperfusion: possible consequences for postischemic recovery. *J Mol Cell Cardiol*. 1989;**21**:1209–18.

30 Potter JD, Robertson SP, Johnson JD. Magnesium and the regulation of muscle contraction. *Fed Proc*. 1981;**40**:2653–6.

31 Ogawa Y. Calcium binding to troponin C and troponin: effects of Mg^{2+}, ionic strength and pH. *J Biochem*. 1985;**97**:1011–23.

32 Zot AS, Potter JD. Structural aspects of troponin-tropomyosin regulation of skeletal muscle contraction. *Annu Rev Biophys Biophys Chem*. 1987;**16**:535–59.

33 Morimoto S. Effect of myosin cross-bridge interaction with Actin on the Ca^{2+}–binding properties of troponin C in fast skeletal myofibrils. *J Biochem*. 1991;**109**:120–6.

34 Francois JM, Gerday C, Prendergast FG, Potter JD. Determination of the Ca^{2+} and Mg^{2+} affinity constants of troponin C from eel skeletal muscle and positioning of the single tryptophan in the primary structure. *J Muscle Res Cell Motil*. 1993;**14**:585–93.

35 She M, Dong WJ, Umeda PK, Cheung HC. Tryptophan mutants of troponin C from skeletal muscle: an optical probe of the regulatory domain. *Eur J Biochem*. 1998;**252**:600–7.

36 Allen TS, Yates LD, Gordon AM. Ca^{2+}-dependence of structural changes in troponin-C in demembranated fibers of rabbit psoas muscle. *Biophys J*. 1992;**61**:399–409.

37 Godt RE, Morgan JL. Contractile responses to MgATP and pH in a thick filament regulated muscle: studies with skinned scallop fibers. *Adv Exp Med Biol*. 1984;**170**:569–72.

38 Godt RE. Calcium-activated tension of skinned muscle fibers of the frog. Dependence on magnesium adenosine triphosphate concentration. *J Gen Physiol*. 1974;**63**:722–39.

39 Best PM, Donaldson SK, Kerrick WG. Tension in mechanically disrupted mammalian cardiac cells: effects of magnesium adenosine triphosphate. *J Physiol*. 1977;**265**:1–17.

40 Davis JP, Rall JA, Reiser PJ, Smillie LB, Tikunova SB. Engineering competitive magnesium binding into the first EF-hand of skeletal troponin C. *J Biol Chem*. 2002;**277**:49716–26.

41 Li AY, Stevens CM, Liang B, Rayani K, Little S, Davis J, et al. Familial hypertrophic cardiomyopathy related cardiac troponin C L29Q mutation alters length-dependent activation and functional effects of phosphomimetic troponin I*. *PLoS ONE*. 2013;**8**:e79363.

42 Holroyde M, Robertson S, Johnson J, Solaro R, Potter J. The calcium and magnesium binding sites on cardiac troponin and their role in the regulation of myofibrillar adenosine triphosphatase. *J Biol Chem*. 1980;**255**:11688–93.

43 Ebashi S, Ogawa Y. Ca^{2+} in contractile processes. *Biophys Chem*. 1988;**29**:137–43.

44 Fabiato A, Fabiato F. Effects of magnesium on contractile activation of skinned cardiac cells. *J Physiol*. 1975;**249**:497–517.

45 Donaldson SK, Kerrick WG. Characterization of the effects of Mg^{2+} on Ca^{2+}- and Sr^{2+}-activated tension generation of skinned skeletal muscle fibers. *J Gen Physiol*. 1975;**66**:427–44.

46 Kerrick WG, Zot HG, Hoar PE, Potter JD. Evidence that the Sr^{2+} activation properties of cardiac troponin C are altered when substituted into skinned skeletal muscle fibers. *J Biol Chem*. 1985;**260**:15687–93.

47 Solaro RJ, Shiner JS. Modulation of Ca^{2+} control of dog and rabbit cardiac myofibrils by Mg^{2+}. Comparison with rabbit skeletal myofibrils. *Circ Res*. 1976;**39**:8–14.

48 Ashley CC, Moisescu DG. Effect of changing the composition of the bathing solutions upon the isometric tension-pCa relationship in bundles of crustacean myofibrils. *J Physiol*. 1977;**270**:627–52.

49 Donaldson SK, Best PM, Kerrick GL. Characterization of the effects of Mg^{2+} on Ca^{2+}- and

Sr^{2+}-activated tension generation of skinned rat cardiac fibers. *J Gen Physiol*. 1978;**71**:645–55.
50 Tanaka H, Takahashi H, Ojima T. Ca^{2+}-binding properties and regulatory roles of lobster troponin C sites II and IV. *FEBS Lett*. 2013;**587**:2612–6.
51 Rayani K, Seffernick J, Li AY, Davis JP, Spuches AM, Van Petegem F, et al. Binding of calcium and magnesium to human cardiac troponin C. *J Biol Chem*. 2021;**296**:100350.
52 Liang B, Chung F, Qu Y, Pavlov D, Gillis TE, Tikunova SB, et al. Familial hypertrophic cardiomyopathy-related cardiac troponin C mutation L29Q affects Ca^{2+} binding and myofilament contractility. *Physiol Genomics*. 2008;**33**:257–66.
53 Tikunova SB, Liu B, Swindle N, Little SC, Gomes AV, Swartz DR, et al. Effect of calcium-sensitizing mutations on calcium binding and exchange with troponin C in increasingly complex biochemical systems. *Biochemistry*. 2010;**49**:1975–84.
54 Gomes AV, Potter JD. Molecular and cellular aspects of troponin cardiomyopathies. *Ann N Y Acad Sci*. 2004;**1015**:214–24.
55 Stevens CM, Rayani K, Singh G, Lotfalisalmasi B, Tieleman DP, Tibbits GF. Changes in the dynamics of the cardiac troponin C molecule explain the effects of Ca^{2+}–sensitizing mutations. *J Biol Chem*. 2017;**292**:11915–26.
56 Ohki S, Ikura M, Zhang M. Identification of Mg^{2+}–binding sites and the role of Mg^{2+} on target recognition by calmodulin. *Biochemistry*. 1997;**36**:4309–16.
57 Malmendal A, Evenas J, Thulin E, Gippert GP, Drakenberg T, Forsen S. When size is important. Accommodation of magnesium in a calcium binding regulatory domain. *J Biol Chem*. 1998;**273**:28994–9001.
58 Andersson M, Malmendal A, Linse S, Ivarsson I, Forsen S, Svensson LA. Structural basis for the negative allostery between Ca(2+)- and Mg(2+)-binding in the intracellular Ca(2+)-receptor calbindin D9k. *Protein Sci*. 1997;**6**:1139–47.
59 Cordina NM, Liew CK, Gell DA, Fajer PG, Mackay JP, Brown LJ. Effects of calcium binding and the hypertrophic cardiomyopathy A8V mutation on the dynamic equilibrium between closed and open conformations of the regulatory N-domain of isolated cardiac troponin C. *Biochemistry*. 2013;**52**:1950–62.
60 Marques MA, Landim-Vieira M, Moraes AH, Sun B, Johnston JR, Jones KMD, et al. Anomalous structural dynamics of minimally frustrated residues in cardiac troponin C triggers hypertrophic cardiomyopathy. *Chem Sci*. 2021;**12**:7308–23.
61 Hoffmann B, Schmidt-Traub H, Perrot A, Osterziel KJ, Gessner R. First mutation in cardiac troponin C, L29Q, in a patient with hypertrophic cardiomyopathy. *Hum Mutat*. 2001;**17**:524.
62 Parvatiyar MS, Landstrom AP, Figueiredo-Freitas C, Potter JD, Ackerman MJ, Pinto JR. A mutation in TNNC1-encoded cardiac troponin C, TNNC1-A31S, predisposes to hypertrophic cardiomyopathy and ventricular fibrillation. *J Biol Chem*. 2012;**287**:31845–55.
63 Landstrom AP, Parvatiyar MS, Pinto JR, Marquardt ML, Bos JM, Tester DJ, et al. Molecular and functional characterization of novel hypertrophic cardiomyopathy susceptibility mutations in TNNC1-encoded troponin C. *J Mol Cell Cardiol*. 2008;**45**:281–8.
64 Gonzalez-Martinez D, Johnston JR, Landim-Vieira M, Ma W, Antipova O, Awan O, et al. Structural and functional impact of troponin C-mediated Ca^{2+} sensitization on myofilament lattice spacing and cross-bridge mechanics in mouse cardiac muscle. *J Mol Cell Cardiol*. 2018;**123**:26–37.
65 van Spaendonck-Zwarts KY, van Tintelen JP, van Veldhuisen DJ, van der Werf R, Jongbloed JD, Paulus WJ, et al. Peripartum cardiomyopathy as a part of familial dilated cardiomyopathy. *Circulation*. 2010;**121**:2169–75.
66 Gillis TE, Marshall CR, Tibbits GF. Functional and evolutionary relationships of troponin C. *Physiol Genomics*. 2007;**32**:16–27.
67 Yamada Y, Namba K, Fujii T. Cardiac muscle thin filament structures reveal calcium regulatory mechanism. *Nat Commun*. 2020;**11**:1–9.
68 Greenberg MJ, Tardiff JC. Complexity in genetic cardiomyopathies and new approaches for mechanism-based precision medicine. *J Gen Physiol*. 2021;**153**: e202012662.
69 Baxley T, Johnson D, Pinto JR, Chalovich JM. Troponin C mutations partially stabilize the active state of regulated Actin and fully stabilize the active state when paired with Δ14 TnT. *Biochemistry*. 2017;**56**:2928–37.
70 Gillis TE, Blumenschein TM, Sykes BD, Tibbits GF. Effect of temperature and the F27W mutation on the Ca^{2+} activated structural transition of trout cardiac troponin C. *Biochemistry*. 2003;**42**:6418–26.
71 Dong W-J, Wang C-K, Gordon AM, Cheung HC. Disparate fluorescence properties of 2-[4′-(Iodoacetamido)anilino]-Naphthalene-6-sulfonic acid attached to Cys-84 and Cys-35 of troponin C in cardiac muscle troponin. *Biophys J*. 1997;**72**:850–7.
72 Freire E, Mayorga OL, Straume M. Isothermal titration calorimetry. *Anal Chem*. 1990;**62**:950A–9A.
73 Pinto JR, Parvatiyar MS, Jones MA, Liang J, Ackerman MJ, Potter JD. A functional and structural study of troponin C mutations related to hypertrophic cardiomyopathy. *J Biol Chem*. 2009;**284**:19090–100.
74 Ramos CH. Mapping subdomains in the C-terminal region of troponin I involved in its binding to

troponin C and to thin filament. *J Biol Chem*. 1999;**274**:18189–95.
75 Risi CM, Pepper I, Belknap B, Landim-Vieira M, White HD, Dryden K, et al. The structure of the native cardiac thin filament at systolic Ca^{2+} levels. *Proc Natl Acad Sci USA*. 2021;**118**:e2024288118.
76 Gifford JL, Walsh MP, Vogel HJ. Structures and metal-ion-binding properties of the Ca^{2+}-binding helix–loop–helix EF-hand motifs. *Biochem J*. 2007;**405**:199–221.
77 Bowman JD, Lindert S. Molecular dynamics and umbrella sampling simulations elucidate differences in troponin C isoform and mutant hydrophobic patch exposure. *J Phys Chem B*. 2018;**122**:7874–83.
78 Zot HG, Hasbun JE, Michell CA, Landim-Vieira M, Pinto JR. Enhanced troponin I binding explains the functional changes produced by the hypertrophic cardiomyopathy mutation A8V of cardiac troponin C. *Arch Biochem Biophys*. 2016;**601**:97–104.
79 Dweck D, Hus N, Potter JD. Challenging current paradigms related to cardiomyopathies are changes in the Ca^{2+} sensitivity of myofilaments containing cardiac troponin C mutations (G159D and L29Q) good predictors of the phenotypic outcomes? *J Biol Chem*. 2008;**283**:33119–28.
80 Pearlstone JR, Borgford T, Chandra M, Oikawa K, Kay CM, Herzberg O, et al. Construction and characterization of a spectral probe mutant of troponin C: application to analyses of mutants with increased calcium affinity. *Biochemistry*. 1992;**31**:6545–53.
81 da Silva AC, de Araujo AH, Herzberg O, Moult J, Sorenson M, Reinach FC. Troponin-C mutants with increased calcium affinity. *Eur J Biochem*. 1993;**213**:599–604.
82 Potluri PR, Cordina NM, Kachooei E, Brown LJ. Characterization of the L29Q hypertrophic cardiomyopathy mutation in cardiac troponin C by paramagnetic relaxation enhancement nuclear magnetic resonance. *Biochemistry*. 2019;**58**:908–17.
83 Johnson JD, Collins JH, Potter JD. Dansylaziridine-labeled troponin C. A fluorescent probe of Ca^{2+} binding to the Ca^{2+}–specific regulatory sites. *J Biol Chem*. 1978;**253**:6451–8.
84 Veltri T, Landim-Vieira M, Parvatiyar MS, Gonzalez-Martinez D, Dieseldorff Jones KM, Michell CA, et al. Hypertrophic cardiomyopathy cardiac troponin C mutations differentially affect slow skeletal and cardiac muscle regulation. *Front Physiol*. 2017;**8**:221.
85 Ward WH, Holdgate GA. 7 isothermal titration calorimetry in drug discovery. *Prog Med Chem*. 2001;**38**:309–76.
86 Wang D, Robertson IM, Li MX, McCully ME, Crane ML, Luo Z, et al. Structural and functional consequences of the cardiac troponin C L48Q Ca^{2+}–sensitizing mutation. *Biochemistry*. 2012;**51**:4473–87.
87 Shettigar V, Zhang B, Little SC, Salhi HE, Hansen BJ, Li N, et al. Rationally engineered troponin C modulates in vivo cardiac function and performance in health and disease. *Nat Commun*. 2016;**7**:10794.
88 Cummins PL, Gready JE. Thermodynamic integration calculations on the relative free energies of complex ions in aqueous solution: application to ligands of dihydrofolate reductase. *J Comput Chem*. 1994;**15**:704–18.
89 Panteva MT, Giambaşu GM, York DM. Comparison of structural, thermodynamic, kinetic and mass transport properties of Mg(2+) ion models commonly used in biomolecular simulations. *J Comput Chem*. 2015;**36**:970–82.
90 Chang AN, Potter JD. Sarcomeric protein mutations in dilated cardiomyopathy. *Heart Fail Rev*. 2005;**10**:225–35.
91 Reid RE, Procyshyn RM. Engineering magnesium selectivity in the helix–loop–helix calcium-binding motif. *Arch Biochem Biophys*. 1995;**323**:115–9.
92 Tikunova SB, Black DJ, Johnson JD, Davis JP. Modifying Mg^{2+} binding and exchange with the N-terminal of calmodulin. *Biochemistry*. 2001;**40**:3348–53.
93 Dai LJ, Friedman PA, Quamme GA. Cellular mechanisms of chlorothiazide and cellular potassium depletion on Mg^{2+} uptake in mouse distal convoluted tubule cells. *Kidney Int*. 1997;**51**:1008–17.
94 Bers DM. Cardiac excitation–contraction coupling. *Nature*. 2002;**415**:198–205.
95 Touyz RM. Reactive oxygen species, vascular oxidative stress, and redox signaling in hypertension: what is the clinical significance? *Hypertension*. 2004;**44**:248–52.
96 Weglicki W, Quamme G, Tucker K, Haigney M, Resnick L. Potassium, magnesium, and electrolyte imbalance and complications in disease management. *Clin Exp Hypertens*. 2005;**27**:95–112.
97 Mazur A, Maier JA, Rock E, Gueux E, Nowacki W, Rayssiguier Y. Magnesium and the inflammatory response: potential physiopathological implications. *Arch Biochem Biophys*. 2007;**458**:48–56.
98 Kolte D, Vijayaraghavan K, Khera S, Sica DA, Frishman WH. Role of magnesium in cardiovascular diseases. *Cardiol Rev*. 2014;**22**:182–92.
99 Murphy E, Steenbergen C, Levy LA, Raju B, London RE. Cytosolic free magnesium levels in ischemic rat heart. *J Biol Chem*. 1989;**264**:5622–7.
100 Stevens CM, Rayani K, Genge CE, Singh G, Liang B, Roller JM, et al. Characterization of zebrafish cardiac and slow skeletal troponin C paralogs by MD simulation and ITC. *Biophys J*. 2016;**111**:38–49.
101 Spyracopoulos L, Li MX, Sia SK, Gagné SM, Chandra M, Solaro RJ, et al. Calcium-induced structural

transition in the regulatory domain of human cardiac troponin C. *Biochemistry*. 1997;**36**:12138–46.
102 Case DA, Betz RM, Cerutti DS, Cheatham TE III, Darden TA, Duke RE, et al. AMBER 2016. San Francisco, CA: University of California; 2016.
103 Maier JA, Martinez C, Kasavajhala K, Wickstrom L, Hauser KE, Simmerling C. ff14SB: improving the accuracy of protein side chain and backbone parameters from ff99SB. *J Chem Theory Comput*. 2015;**11**:3696–713.
104 Li P, Roberts BP, Chakravorty DK, Merz KM. Rational design of particle mesh Ewald compatible Lennard-Jones parameters for +2 metal cations in explicit solvent. *J Chem Theory Comput*. 2013;**9**:2733–48.
105 Essmann U, Perera L, Berkowitz ML, Darden T, Lee H, Pedersen LG. A smooth particle mesh Ewald method. *J Chem Phys*. 1995;**103**:8577–93.
106 Leelananda SP, Lindert S. Computational methods in drug discovery. *Beilstein J Org Chem*. 2016;**12**:2694–718.
107 Shirts MR, Chodera JD. Statistically optimal analysis of samples from multiple equilibrium states. *J Chem Phys*. 2008;**129**:124105.
108 DeLano, W. L. The PyMOL Molecular Graphics System, Schrödinger, LLC. Palo Alto, CA: DeLano Scientific LLC; 2002.
109 Takeda S, Yamashita A, Maeda K, Maéda Y. Structure of the core domain of human cardiac troponin in the Ca(2+)-saturated form. *Nature*. 2003;**424**:35–41.

Supporting information

Additional supporting information may be found online in the Supporting Information section at the end of the article.

Figure S1 Representative isotherms are presented to quantify the heat signal from the interaction with each of Ca^{2+} and Mg^{2+} with the buffer. N-values do not present any utility and are included for completeness. The buffer titrations involve only transient binding interactions such as hydrogen bonds and Van der Waals forces if indeed they are quantifiable, between the solutes and solvents; this system contains no protein and no true binding sites. The scale may be used as measure of the heat change in the system and a proxy to compare with the titrant into N-cTnC conditions. The values measured when a single binding site model was used to fit each titration are presented in the table.